

Microburst Scale Size Distribution Derived with AeroCube-6

M. Shumko¹, T.P. O’Brien², J. Sample¹, A. Johnson¹, D.L. Turner², J.B.
Blake², B.A. Griffith¹, S. Claudepierre², O. Agapitov³

¹Department of Physics, Montana State University, Bozeman, Montana, USA

²Space Science Applications Laboratory, The Aerospace Corporation, El Segundo, California, USA

³Space Sciences Laboratory, University of California Berkeley, Berkeley, California, USA

Key Points:

- Microburst scale size in low Earth orbit and the magnetic equator was estimated.
- Majority of microbursts in low Earth orbit have a scale size on the order of 10 km.
- The majority of microbursts correspond to the correlation scale of **high amplitude?** whistler-mode chorus waves at the magnetic equator.

Corresponding author: M. Shumko, msshumko@gmail.com

Abstract

Microbursts are an impulsive increase of electrons from the radiation belts into the atmosphere and has been directly observed in low Earth orbit and upper atmosphere. Microbursts are believed to be generated by wave-particle scattering between whistler mode waves and radiation belt electrons. Prior work has estimated that microbursts are capable of rapidly depleting the radiation belt electrons on the order of a day, hence their role to radiation belt electron losses must be considered. Radiation belt electron losses due to microbursts is not well understood, and more work is necessary to accurately quantify their contribution. To further address this question we present a statistical study of microburst scale sizes using the pair of AeroCube-6 CubeSats. The microburst scale size distribution in low Earth orbit and the magnetic equator was derived. In low Earth orbit, the majority of microbursts were found to have a size of less than a few tens of km with a minority of microbursts observed at a separation above 50 km. When mapped to the magnetic equator, the microburst scale size distribution corresponded to the high amplitude whistler mode chorus scale size derived in prior literature.

1 Plain Language Summary

<https://sharingscience.agu.org/creating-plain-language-summary/>

2 Introduction

Since the discovery of the Van Allen radiation belts in the 1960s by Van Allen (1959) and Vernov and Chudakov (1960), decades of research has made headway in understanding the dynamics of particle acceleration and loss mechanisms. One of these mechanisms is wave-particle scattering between whistler-mode chorus waves and electrons which has been modeled and observed as a source of electron acceleration and loss (Abel & Thorne, 1998; Meredith et al., 2002; Horne & Thorne, 2003; Thorne et al., 2005; Millan & Thorne, 2007; Bortnik et al., 2008). Whistler-mode chorus waves are typically generated by a temperature anisotropy of low energy electrons up to tens of kiloelectronvolts (keV) (Li, Thorne, Angelopoulos, Bonnell, et al., 2009). Li, Thorne, Angelopoulos, Bortnik, et al. (2009) found that chorus waves predominately occur in ~ 6 – 12 magnetic local times (MLT).

Whistler mode chorus is widely believed to cause electron precipitation termed microbursts (Millan & Thorne, 2007). Microbursts are a subsecond impulse of electrons that are observed by high altitude balloons and satellites in low Earth orbit (LEO) on the radiation belt magnetic footprints, ~ 4 – 8 L-shell (L) (Anderson & Milton, 1964; Parks, 1967; Woodger et al., 2015; Lorentzen, Blake, et al., 2001; Lorentzen, Looper, & Blake, 2001; O'Brien et al., 2003, 2004; Lee et al., 2005, 2012; Crew et al., 2016; Breneman et al., 2017; Mozer et al., 2018). Microbursts role as a radiation belt electron loss mechanism has been estimated to be significant, with total radiation belt electron depletion due to microbursts estimated to be on the order of a day (Lorentzen, Looper, & Blake, 2001; O'Brien et al., 2004; Thorne et al., 2005; Breneman et al., 2017).

One of the unknown characteristics of microbursts that is critical to better quantify the role of microbursts as a loss mechanism is their size. Move "why we should care?" to end of paragraph? Microburst size, together with their occurrence frequency anything else? are necessary parameters to more accurately quantify their contribution to radiation belt electron losses. Furthermore, by comparing the microburst scale size distribution mapped to the magnetic equator to the wave scale sizes estimated in prior literature, the dominant scattering mechanism can be identified. Historically there have been various case studies that estimated microburst scale size. Parks (1967) found that the scale size of mostly low energy microbursts to be 40 ± 14 km. Blake et al. (1996) found a microburst with a size of a few tens of km using the the Solar Anomalous and Magnetospheric Particle Explorer (SAMPEX) and concluded that typically microbursts

are less than a few tens of electron gyroradii in size (order of a few km). Dietrich et al. (2010) also used SAMPEX in another case study and concluded that the observed microbursts were smaller than 4 km. More recently, Crew et al. (2016) used the Focused Investigation of Relativistic Electron Bursts: Intensity, Range, and Dynamics CubeSats and found an example of a microburst larger than 11 km, and Shumko et al. (2018) found a microburst with a size greater than 51 ± 1 km. The large variance in prior results imply that there is a distribution of microburst scale sizes that this study aims to estimate.

This study estimates the microburst scale size distributions in LEO and the magnetic equator and compares it to the scale size of the progenitor waves. The twin AeroCube-6 (AC6) CubeSats which took data together for three years with varying spacecraft separation between 2 and 800 km are utilized for this study. We first introduce the AC-6 mission including their orbit and instrumentation. Then we describe the procedure undertaken to identify microbursts observed by each spacecraft and how they are combined to make a list of the temporally coincident microbursts. Next, the procedure used to estimate the microburst scale size distributions in LEO and the magnetic equator is explained. Lastly, we summarize and compare these results to the microburst scale sizes estimated in prior literature and infer the properties of the whistler-mode chorus waves that are believed to cause microbursts.

3 Instrumentation

The AC6 mission consists of a pair of 0.5U (10x10x5 cm) CubeSats built by the Aerospace Corporation and launched on June 19th, 2014 into a 620 x 700 km, 98 degree inclination orbit. The two satellites, designated as AC6-A and AC6-B separated after launch and drifted apart. AC6 has an active attitude control system which allows them to change their differential drag to allow fine separation control. Figure 1a shows the AC6 separation for the duration of the mission.

Each AC6 unit is equipped with a three Aerospace microdosimeters (licensed to Teledyne Microelectronics, Inc). The dosimeter used for this study is dos1 and is identical on both AC6 units. Dos1 has a 30 keV electron threshold and samples at 10 Hz. The AC6 orbit is in the dawn-dusk magnetic local times (MLTs) and Fig. 1b shows the number of good 10 Hz samples taken simultaneously by AC6 as a function of L and MLT. Good samples are samples which have a 0 data quality flag. More detailed technical information regarding the AC6 mission can be found in O'Brien et al. (2016).

4 Methodology

4.1 Microburst Detection

The first step to find microbursts observed simultaneously by both spacecraft is to identify them from each spacecraft separately. We have detected microbursts with two different methods that yielded quantitatively similar results. The first method is the burst parameter cite Pauls paper and add equation. This algorithm has been successfully used in other microburst studies, mainly with the microbursts observed by the Solar Anomalous and Magnetospheric Particle Explorer add citations. For AC6, we found that a burst parameter threshold of 5 has good tradeoff between false positive and false negative microburst detections.

Maybe not go into as much in detail in the following paragraph? The other microburst detection algorithm that was developed for this study is based on wavelet transforms and frequency filtering cite Torrence and Compo. The AC6 time series is first transformed into wavelet space by convolving it with a set of Ricker wavelets (more commonly known as the Mexican hat wavelet). An example of the wavelet transformation is shown in Fig. 2. Figure 2a shows the original time series in blue for one radiation belt pass and Fig.

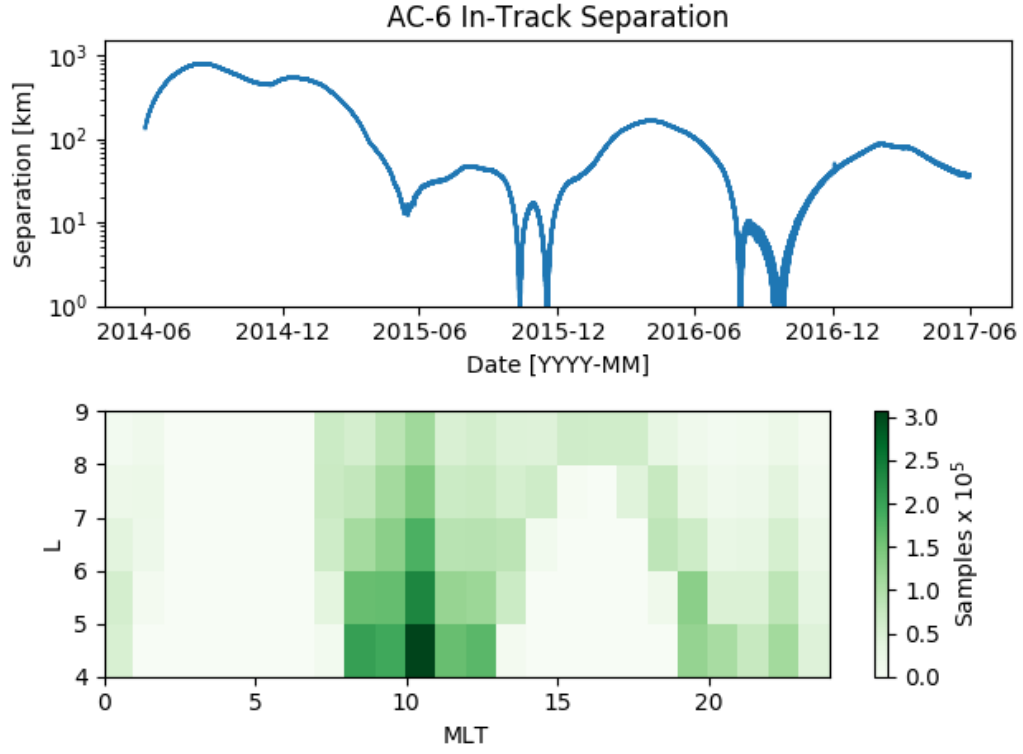


Figure 1. AC6 mission distributions for (a) spacecraft separation and (b) number of simultaneous 10 Hz samples as a function of L and MLT.

2b shows the wavelet power as a function of period of oscillation and time. At times when microbursts were observed, there is substantial wavelet power in periods less than one second.

A high pass filter at one second was then applied on the wavelet space representation of the microburst time series. Then the remaining wavelet space was inverse filtered to produce a time series which is zero or near-zero everywhere except microbursts. Lastly, a threshold test was applied to identify microbursts. Example detections of microbursts are shown with green stars in Fig. 2a.

4.2 Transmitter Noise Removal

The transmitters on AC6 can cause unphysical count impulses in the dosimeters. One source of transmitter noise was observed at times when AC6 was in contact with the ground stations above mainland US for data downloads and commanding. This source of noise mainly manifests itself at lower radiation belt L shells. To account for this noise, detections made above the US were discarded.

Another source of noise is crosslink transmissions between the AC6 units. These transmissions occurred when either spacecraft transitioned from the survey mode to 10 Hz mode. This noise is often not caught by the data quality flag, so an automated noise identification process was developed. To identify this noise, a dosimeter with a 250 keV nominal electron threshold, dos2 was used. Dos2 typically has negligible count rates when dos1 is observing microbursts, and substantial count rates during downlinks and crosslinks. Furthermore, the crosslink transmissions are relatively easy to identify since they are observed near the start and end of the 10 Hz data periods, and are very periodic. The automated noise identification algorithm applied cross-correlation (CC) and autocorrelation (AC) to the dos1 and dos2 time series. Microburst detections were removed when the following two conditions were met. The first condition is true if the dos1 or dos2 time series had an AC peak at 0.2 or 0.4 s lag. The second condition is true if dos2 observed unphysically high count rates or dos1 and dos2 had a Pearson CC coefficient < 0.9 . The first condition can be met with a train of microbursts alone and to not remove these valid detections, we imply a second constraint that dos2 experiences unphysical counts or dos1 and dos2 well cross correlate which is unlikely due to an order of magnitude difference in dos1 and dos2 energy thresholds. This admittedly complex algorithm successfully removed most transmitter noise while preserving most valid microburst detections.

4.3 Coincident Microburst Detection

At this stage we have lists of microbursts observed by both spacecraft individually and now we combine these lists to identify microbursts observed simultaneously by both AC6 units. Show the microburst detection schematic? The general approach is to CC the time series around microbursts detections made by one spacecraft against the other spacecraft. Ideally, if both spacecraft observed the same microburst, the two time series should correlate well and correlate poorly when a microburst is correlated against random non-microburst times. A CC threshold of 0.8 was chosen as it is a good compromise to identify microbursts superposed with noise and rejecting moderate correlations between a microburst and random features in the other time series. This CC threshold sometimes failed to reject times when microbursts and non-microburst features were well correlated due to Poisson noise so all of the events were spot checked by two authors to remove these events. All things considered, 662 confirmed microburst detections are used to calculate the microburst scale size distribution in the following section. Figure 3, panels (a), (c), and (e) show examples of microbursts observed by both AC6 units when they were separated by 6, 17, and 69 km, respectively.

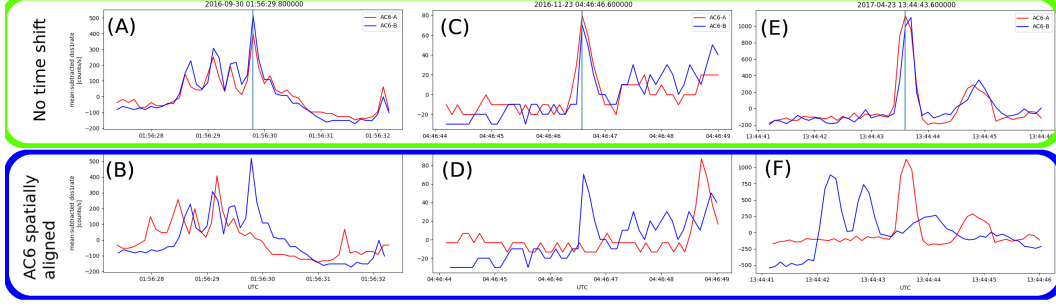


Figure 2. Examples of microbursts observed simultaneously by AC6. Panels (a), (c) and (e) shows the temporally-aligned time series at spacecraft separations of 5.6 km, 16.5 km, and 68.5 km, respectively. Panels (b), (d), and (f) show the spatially aligned time series corresponding to the time series in the same column. The clear temporal correlation and lack of spatial correlation demonstrates that these events are microbursts.

A physical phenomena that can influence our results are narrow spatial structures termed curtains cite Bern and Pauls paper. These structures appear as microbursts in a time series from a single satellite, but with two satellites you can adjust the time series of one spacecraft by the in-track lag to identify spatial features. Figure 3b, d, and f show the AC6 spatially aligned time series and show that the these three cases were indeed microbursts.

When the two spacecraft were as little as a few kilometers apart it is very difficult to distinguish between temporal features such as microbursts from spatial features such as curtains. Since the prevalence of curtains is independent of the spacecraft separation, this will effectively reduce the number of microbursts observed at very small separations. No attempt has been made to remove this bias.

4.4 Microburst Size Distribution in LEO and Magnetic Equator

When AC6 observes a coincident microburst at a separation d , the microburst's size must be greater than d . This idea is similar to Joy et al. (2002) who investigated the most probable Jovian bow shock and magnetopause standoff distances. Following the arguments presented in Section 4 in Joy et al. (2002), we investigate the dependence of the number of coincident microbursts observed above d , as a function of d that is the microburst complementary cumulative distribution $F(d)$. If $P(A)$ is the probability that a microburst is larger than d and $P(B)$ is the probability that AC6 is separated by d , then the fraction of microbursts observed at d is the conditional probability $P(A | B)$. Using Bayes theorem,

$$P(A | B) = \frac{P(A \& B)}{P(B)} \quad (1)$$

where $P(A \& B)$ is the joint probability. Since the AC6 separation is independent of microburst size, $P(A \& B) = P(A)P(B)$. Hence

$$P(A | B) = \frac{P(A)P(B)}{P(B)} = P(A) \quad (2)$$

and seems like a big jump in logic...

$$F(d) = \frac{N(d)}{N(0)} \quad (3)$$

where $N(d)$ is the number of microbursts observed by AC6 above separation d and is defined as

$$N(d) = \sum_{\text{bins} > d} n_{\text{bin}} \frac{S_{\text{max}}}{S_{\text{bin}}} \quad (4)$$

where n_{bin} is the number of microbursts detected by both AC6 units in that bin. The normalization term $S_{\text{max}}/S_{\text{bin}}$ is a ratio of the number of samples observed in the most sampled bin to the number of samples in the current bin. This normalization factor corrects for AC6's non-uniform sampling in separation. With this normalization, $F(d)$ can be interpreted as the fraction of microbursts observed above d assuming AC6 sampled evenly in separation. Microburst $F(d)$ in LEO is shown by the black curve in Fig. 3a for the entire radiation belt ($4 < L < 8$) and split into one L -wide bins with the colored curves. The separation bin width in Fig. 3 is 5 km. To check for bias in $F(d)$ due to the separation bins, other bin widths and offsets were used to calculate $F(d)$. Bin widths as large as the size of the features in $F(d)$ (20–30 km) and bin offsets smaller than the bin width did not effect the curves in Fig. 3a.

The overall trend in Fig. 3a consists of a sudden cumulative probability drop off, followed by a shoulder up to about 70 km where the cumulative distribution drops to zero. The shaded region around the black curve shows the standard error due to counting statistics. The uncertainty due to false coincidence events i.e. two unrelated microbursts randomly lining up in time was also considered. For each coincident microburst the microburst duty cycle in a one minute window ($\approx 1L$) was calculated. The false coincidence probability is then the square of the duty cycle and was found to be less than 5% for the majority of these events. The false coincidence probability for each microburst was then used to randomly remove microbursts and $F(d)$ was recalculated in 1000 trials. The uncertainty in $F(d)$ with microbursts randomly removed was much smaller than the uncertainty due to counting statistics alone. Lastly, Fig. 3b shows the microburst probability density derived numerically from $F(d)$ and shows a peak at $d < 20$ km as well as a peak between 70-80 km that is **not statistically significant**.

To estimate the equatorial microburst scale size distribution, the microburst events were mapped to the magnetic equator using the Olson-Pfitzer magnetic field model (Olson & Pfitzer, 1982) which is implemented with a Python wrapper for IRBEM-Lib (Boscher et al., 2012). Then the procedure to estimate $F(d)$ is identical to the LEO scale size distribution. One distinction is the normalization. The normalization factors were calculated by mapping every AC6 time series sample taken simultaneously, to the magnetic equator and binning them by separation into 100 km wide, and one L wide bins. Figure 4 shows the equatorial microburst scale size distribution in the same format as Fig. 3. Similar to the microburst probability density in LEO, there is a peak for microburst of sizes less than 200 km and a secondary **not statistically significant** peak at 1200-1600 km.

5 Modeling Microburst Size

TO-DO

- Show a LEO CDF model assuming a fixed-sized microburst population.
- Decide if I should show a two-fixed-sized microburst population or a microburst CDF.
- Think about other distributions e.g. gamma, log-normal, Weibull, Extreme Value Distribution, or Skew normal.
- Show the residuals in the plots.

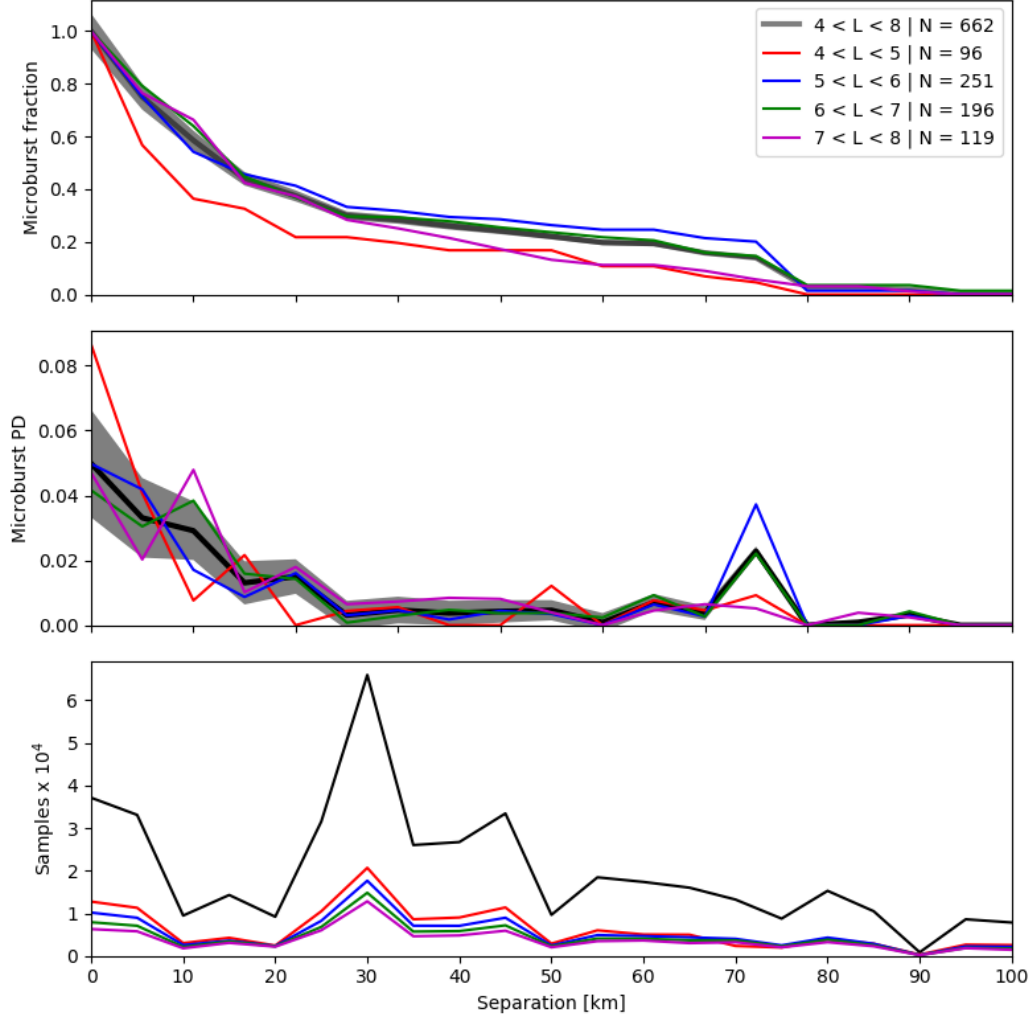


Figure 3. Microburst scale size distribution in LEO. Panel (a) shows the microburst complementary cumulative distribution as a function of spacecraft separation. The complementary cumulative distribution at separation d can be interpreted as the fraction of microbursts observed above d . Panel (b) shows the microburst probability density as a function of separation. Lastly, panel (c) shows the number of simultaneous samples AC6 observed as a function of separation. The colored lines show the distributions broken up by L , and the thick black line shows the overall cumulative distribution in the radiation belt ($4 < L < 8$). The gray shading shows the uncertainty due to counting statistics. change xlabel to spacecraft separation

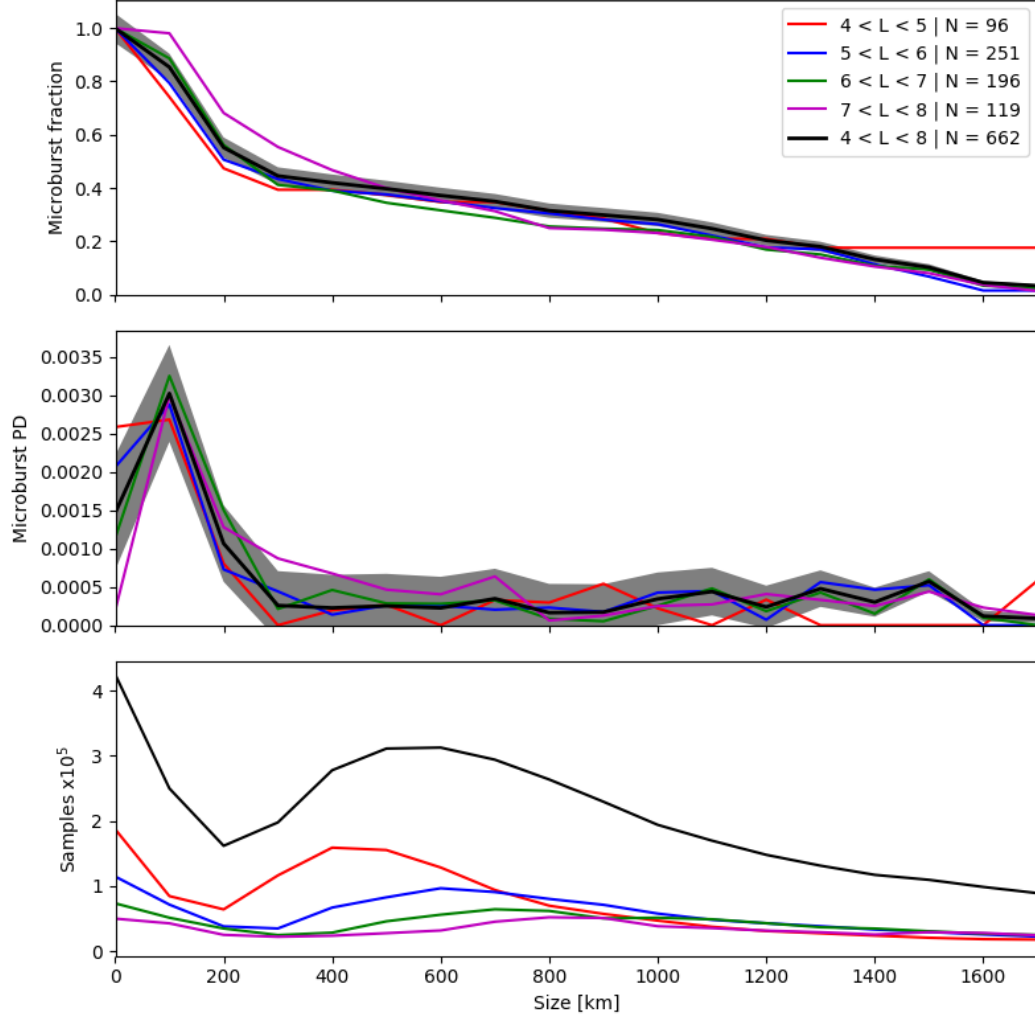


Figure 4. Microburst scale size distribution in the same format as Fig. 3 and mapped to the magnetic equator.

In this section we discuss the model developed to understand the relation between $F(d)$ shown in Fig. 3a and the true distribution of microburst sizes. This relation is not immediately clear since microbursts are randomly scattered around the spacecraft location during a radiation belt pass, and have an unknown geometry. We address these issues with a Monte Carlo (MC) and analytic models and we assume that microbursts are circular with a radius r . For simplicity we first assume that all microbursts are the same r and then generalize their size to a microburst probability density function (PDF).

The MC model first randomly scattered 10^5 microburst centers in a 400 x 400 km grid around the spacecraft. Spacecraft A is placed at the origin, and spacecraft B is placed along the positive y-axis at the same distances from the origin as the separation bins, D used in Section 4.4. Then the number of simultaneously observed microbursts at each spacecraft B distance in D was counted. The modeled fraction of microbursts is then

$$F(d) = \frac{\sum_{d>D} n_d}{\sum_{d \in D} n_d}. \quad (5)$$

and an example run of the MC model with a 40 km diameter microburst population is shown in Fig. 5b.

The analytic model, while identical to the MC model, highlights the concepts connecting the microburst size distribution and $F(d)$. The fundamental idea is that given a spacecraft separation d and microburst radius r , there exists an area A with the property that for any microburst center inside it will be observed by both spacecraft. The geometry of this model and A is shown in Fig. 5a. Figure 5a shows the two spacecraft as blue cubes and two identical microbursts of radius r shown by the black circles. This extreme case shows that the microburst centers are r from either spacecraft, the maximum distance away from the spacecraft and be observed by both units. Microbursts with centers closer to the spacecraft will also be observed by both spacecraft.

Now we use the original geometry and rotate the right circle clockwise about the top spacecraft until the bottom spacecraft is outside the rotated circle. The circle's origin will trace a curve that connects the two black circle centers which is shown by the lower red-dotted line. This problem is symmetric and we can also rotate the right circle counter-clockwise about the lower spacecraft in the same manner and the center will trace out the upper red-dotted curve. The two red-dotted lines outline A and if a microburst center lies anywhere in A , it will be observed by both spacecraft.

How do we find A ? It must be a function of r and d and we need to find $A(r, d)$. Instead of tracing out the red-dotted curves between the black circles' centers, the black circles are rotated through a full revolution. This will trace out the circles comprised of the red and red-dotted curves. These centers of the two circles are separated by d and the radius of the circles is r and A is the area where the two circles intersect and is given by

$$A(r, d) = 2r^2 \cos^{-1} \left(\frac{d}{2r} \right) - \frac{d}{2} \sqrt{4r^2 - d^2}. \quad (6)$$

Cite anything? Wolfram: <http://mathworld.wolfram.com/Circle-CircleIntersection.html>
Lastly, the fraction of microbursts as a function of separation is given by

$$F(r, d) = \frac{\sum_{d>D} A(r, d)}{\sum_{d \in D} A(r, d)}. \quad (7)$$

Where the denominator is the normalization factor. An example of the analytic $F(r = 20 \text{ km}, d)$ is shown in Fig. 5b with the dashed blue curve. The modeled $F(d)$ fits the initial falloff very well, but greatly departs around 20 km that is indicative that there is a distribution of microburst sizes and not all microbursts are the same size. Furthermore

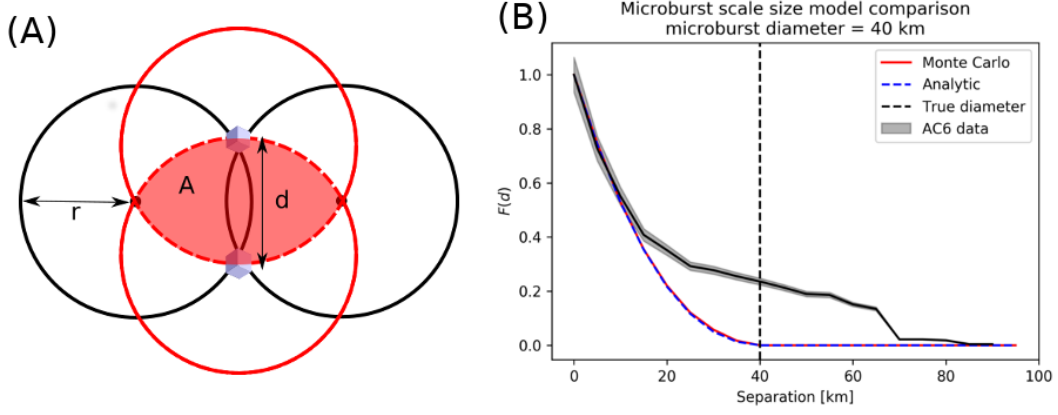


Figure 5. Modeling a one-sized microburst distribution. Panel A shows the geometry of the analytic model. Assuming a microburst radius r (microbursts shown with black circles) and spacecraft separation d , the area A shows all possible microburst center locations where a microburst will be simultaneously observed by both spacecraft. The two black circles show the most distant microburst location that is observed by both spacecraft. The red solid and dashed curves are found by rotating either of the black circles about the top and bottom spacecraft. Panel B shows the microburst fraction, $F(d)$ as a function of separation from the AC6 data in solid black. The red and dashed blue curves show the $F(d)$ assuming all microbursts have a 40 km diameter.

this toy model illustrates the effect that randomly scattered microbursts have on interpreting the results.

To expand on the one-sized microburst results, a two-sized microburst distribution model was developed. The microburst PDF is modeled as

$$f(d, d_1, d_2, a) = a\delta(d - d_1) + (1 - a)\delta(d - d_2) \quad (8)$$

where δ is the Dirac delta function, d_1 and d_2 are the two microburst sizes, and a is the microburst population mixing i.e. fraction term.

6 Discussion

TO-DO

- Discuss the significance of the peaks in the LEO CDF & PDF.
- Discuss the secondary peak.
- Talk about how these sizes fit in with prior work and how they can be used to estimate microburst loss rates.
- Maybe add a plot with Oleksiy's data?
- Use the wave data to interpret the equatorial scale size distribution. Is the 200 km peak due to high amplitude waves, or is it just that waves are most common at those scales?

7 Conclusions

Acknowledgments

Enter acknowledgments, including your data availability statement, here.

References

- Abel, B., & Thorne, R. M. (1998). Electron scattering loss in earth's inner magnetosphere: 1. dominant physical processes. *Journal of Geophysical Research: Space Physics*, 103(A2), 2385–2396.
- Anderson, K. A., & Milton, D. W. (1964). Balloon observations of X rays in the auroral zone: 3. High time resolution studies. *Journal of Geophysical Research*, 69(21), 4457–4479. Retrieved from <http://dx.doi.org/10.1029/JZ069i021p04457> doi: 10.1029/JZ069i021p04457
- Blake, J., Looper, M., Baker, D., Nakamura, R., Klecker, B., & Hovestadt, D. (1996). New high temporal and spatial resolution measurements by sampex of the precipitation of relativistic electrons. *Advances in Space Research*, 18(8), 171–186. Retrieved from <http://www.sciencedirect.com/science/article/pii/0273117795009698> doi: [http://dx.doi.org/10.1016/0273-1177\(95\)00969-8](http://dx.doi.org/10.1016/0273-1177(95)00969-8)
- Bortnik, J., Thorne, R., & Inan, U. S. (2008). Nonlinear interaction of energetic electrons with large amplitude chorus. *Geophysical Research Letters*, 35(21).
- Boscher, D., Bourdarie, S., O'Brien, P., Guild, T., & Shumko, M. (2012). *Irbem-lib library*.
- Breneman, A., Crew, A., Sample, J., Klumpar, D., Johnson, A., Agapitov, O., ... others (2017). Observations directly linking relativistic electron microbursts to whistler mode chorus: Van allen probes and FIREBIRD II. *Geophysical Research Letters*.
- Crew, A. B., Spence, H. E., Blake, J. B., Klumpar, D. M., Larsen, B. A., O'Brien, T. P., ... Widholm, M. (2016). First multipoint in situ observations of electron microbursts: Initial results from the NSF FIREBIRD II mission. *Journal of Geophysical Research: Space Physics*, 121(6), 5272–5283. Retrieved from <http://dx.doi.org/10.1002/2016JA022485> (2016JA022485) doi: 10.1002/2016JA022485
- Dietrich, S., Rodger, C. J., Clilverd, M. A., Bortnik, J., & Raita, T. (2010). Relativistic microburst storm characteristics: Combined satellite and ground-based observations. *Journal of Geophysical Research: Space Physics*, 115(A12).
- Horne, R. B., & Thorne, R. M. (2003). Relativistic electron acceleration and precipitation during resonant interactions with whistler-mode chorus. *Geophysical Research Letters*, 30(10). Retrieved from <http://dx.doi.org/10.1029/2003GL016973> (1527) doi: 10.1029/2003GL016973
- Joy, S., Kivelson, M., Walker, R., Khurana, K., Russell, C., & Ogino, T. (2002). Probabilistic models of the jovian magnetopause and bow shock locations. *Journal of Geophysical Research: Space Physics*, 107(A10), SMP–17.
- Lee, J. J., Parks, G. K., Lee, E., Tsurutani, B. T., Hwang, J., Cho, K. S., ... McCarthy, M. P. (2012). Anisotropic pitch angle distribution of 100 keV microburst electrons in the loss cone: measurements from STSAT-1. *Annales Geophysicae*, 30(11), 1567–1573. Retrieved from <https://www.ann-geophys.net/30/1567/2012/> doi: 10.5194/angeo-30-1567-2012
- Lee, J.-J., Parks, G. K., Min, K. W., Kim, H. J., Park, J., Hwang, J., ... Park, H. Y. (2005). Energy spectra of 170–360 keV electron microbursts measured by the korean STSAT-1. *Geophysical Research Letters*, 32(13). Retrieved from <http://dx.doi.org/10.1029/2005GL022996> (L13106) doi: 10.1029/2005GL022996
- Li, W., Thorne, R., Angelopoulos, V., Bonnell, J., McFadden, J., Carlson, C., ... Auster, H. (2009). Evaluation of whistler-mode chorus intensification on the nightside during an injection event observed on the THEMIS spacecraft. *Journal of Geophysical Research: Space Physics*, 114(A1).
- Li, W., Thorne, R. M., Angelopoulos, V., Bortnik, J., Cully, C. M., Ni, B., ... Magnes, W. (2009). Global distribution of whistler-mode chorus waves observed on the THEMIS spacecraft. *Geophysical Research Letters*, 36(9).

- Retrieved from <http://dx.doi.org/10.1029/2009GL037595> (L09104) doi: 10.1029/2009GL037595
- Lorentzen, K. R., Blake, J. B., Inan, U. S., & Bortnik, J. (2001). Observations of relativistic electron microbursts in association with VLF chorus. *Journal of Geophysical Research: Space Physics*, 106(A4), 6017–6027. Retrieved from <http://dx.doi.org/10.1029/2000JA003018> doi: 10.1029/2000JA003018
- Lorentzen, K. R., Looper, M. D., & Blake, J. B. (2001). Relativistic electron microbursts during the GEM storms. *Geophysical Research Letters*, 28(13), 2573–2576. Retrieved from <http://dx.doi.org/10.1029/2001GL012926> doi: 10.1029/2001GL012926
- Meredith, N., Horne, R., Summers, D., Thorne, R., Iles, R., Heynderickx, D., & Anderson, R. (2002). Evidence for acceleration of outer zone electrons to relativistic energies by whistler mode chorus. In *Annales geophysicae* (Vol. 20, pp. 967–979).
- Millan, R., & Thorne, R. (2007). Review of radiation belt relativistic electron losses. *Journal of Atmospheric and Solar-Terrestrial Physics*, 69(3), 362–377. Retrieved from <http://www.sciencedirect.com/science/article/pii/S1364682606002768> doi: <http://dx.doi.org/10.1016/j.jastp.2006.06.019>
- Mozer, F. S., Agapitov, O. V., Blake, J. B., & Vasko, I. Y. (2018). Simultaneous observations of lower band chorus emissions at the equator and microburst precipitating electrons in the ionosphere. *Geophysical Research Letters*. Retrieved from <http://dx.doi.org/10.1002/2017GL076120> doi: 10.1002/2017GL076120
- O'Brien, T. P., Blake, J. B., & W., G. J. (2016, May). *Aerocube-6 dosimeter data readme* (Tech. Rep. No. TOR-2016-01155). The Aerospace Corporation.
- O'Brien, T. P., Looper, M. D., & Blake, J. B. (2004). Quantification of relativistic electron microburst losses during the GEM storms. *Geophysical Research Letters*, 31(4). Retrieved from <http://dx.doi.org/10.1029/2003GL018621> (L04802) doi: 10.1029/2003GL018621
- O'Brien, T. P., Lorentzen, K. R., Mann, I. R., Meredith, N. P., Blake, J. B., Fennell, J. F., ... Anderson, R. R. (2003). Energization of relativistic electrons in the presence of ULF power and MeV microbursts: Evidence for dual ULF and VLF acceleration. *Journal of Geophysical Research: Space Physics*, 108(A8). Retrieved from <http://dx.doi.org/10.1029/2002JA009784> doi: 10.1029/2002JA009784
- Olson, W. P., & Pfizter, K. A. (1982). A dynamic model of the magnetospheric magnetic and electric fields for July 29, 1977. *Journal of Geophysical Research: Space Physics*, 87(A8), 5943–5948. Retrieved from <http://dx.doi.org/10.1029/JA087iA08p05943> doi: 10.1029/JA087iA08p05943
- Parks, G. K. (1967). Spatial characteristics of auroral-zone X-ray microbursts. *Journal of Geophysical Research*, 72(1), 215–226.
- Shumko, M., Sample, J., Johnson, A., Blake, B., Crew, A., Spence, H., ... Handley, M. (2018). Microburst scale size derived from multiple bounces of a microburst simultaneously observed with the firebird-ii cubesats. *Geophysical Research Letters*, 45(17), 8811–8818. Retrieved from <https://agupubs.onlinelibrary.wiley.com/doi/abs/10.1029/2018GL078925> doi: 10.1029/2018GL078925
- Thorne, R. M., O'Brien, T. P., Shprits, Y. Y., Summers, D., & Horne, R. B. (2005). Timescale for MeV electron microburst loss during geomagnetic storms. *Journal of Geophysical Research: Space Physics*, 110(A9). Retrieved from <http://dx.doi.org/10.1029/2004JA010882> (A09202) doi: 10.1029/2004JA010882
- Van Allen, J. A. (1959). The geomagnetically trapped corpuscular radiation. *Journal of Geophysical Research*, 64(11), 1683–1689. Retrieved from <http://dx.doi.org/10.1029/JZ064i011p01683> doi: 10.1029/JZ064i011p01683
- Vernov, S., & Chudakov, A. (1960). Investigation of radiation in outer space. In *In-*

398 *ternational cosmic ray conference* (Vol. 3, p. 19).
399 Woodger, L., Halford, A., Millan, R., McCarthy, M., Smith, D., Bowers, G., . . .
400 Liang, X. (2015). A summary of the BARREL campaigns: Technique for
401 studying electron precipitation. *Journal of Geophysical Research: Space*
402 *Physics*, 120(6), 4922–4935.